a

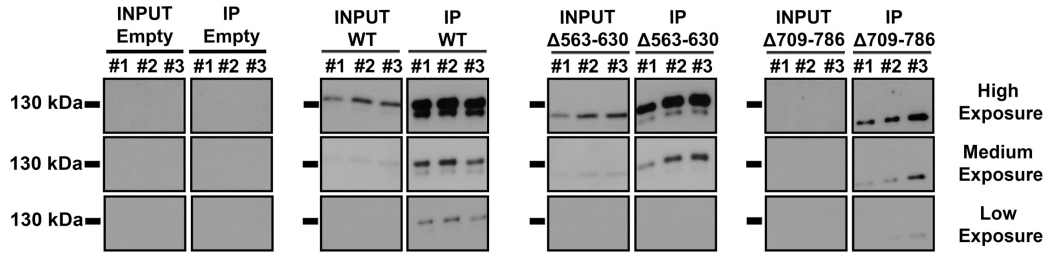

b

Sample	RNA Concentration, pg/µl
IP Empty #1	155.4
IP Empty #2	220
IP Empty #3	148.2
IP AKAP WT #1	8800
IP AKAP WT #2	7680
IP AKAP WT #3	8280
IP Δ563-630 #1	128.6
IP Δ563-630 #2	492
IP Δ563-630 #3	204
IP Δ709-786 #1	1288
IP Δ709-786 #2	926
IP Δ709-786 #3	1028

c

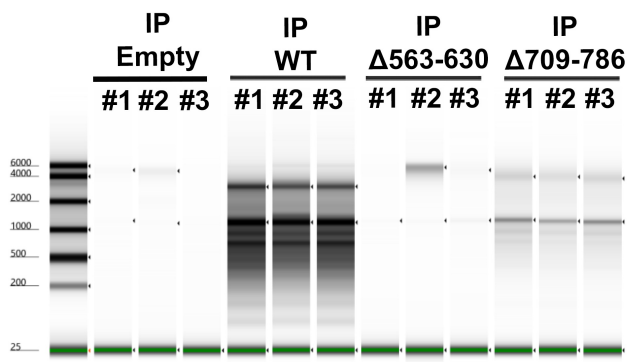

d

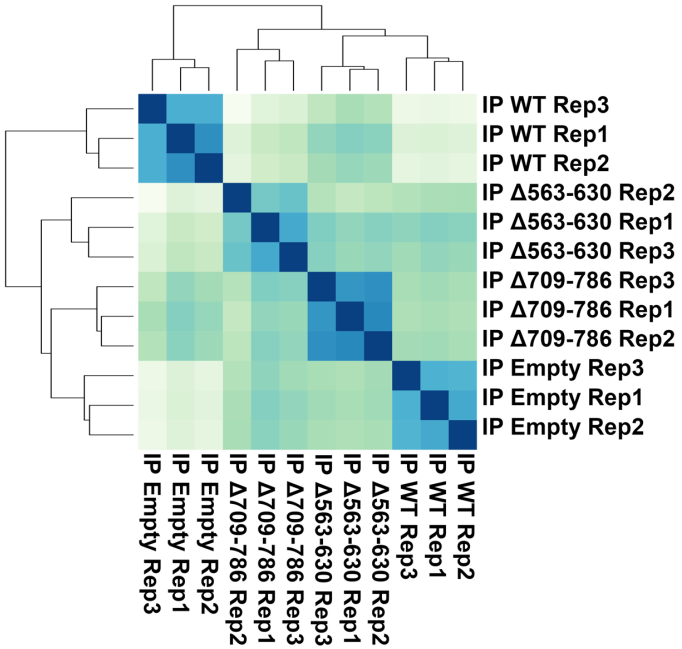

e

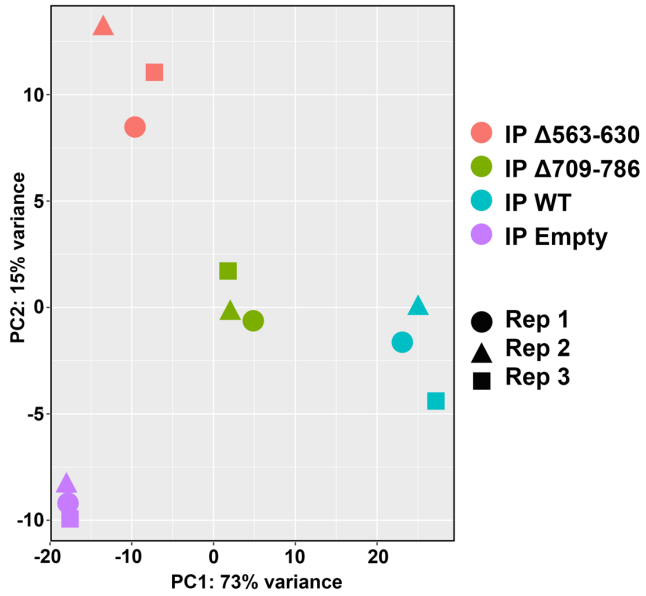

Supplementary Figure 1 (A) Immunoblot analysis of total lysates and V5 IP from U87MG cells transiently expressing V5-tagged WT AKAP1, Δ563–630, or Δ709–786 deletion mutants. IP was performed using an anti-V5 antibody, and both input and IP fractions were probed with anti-V5 to assess protein expression levels and IP efficiency. (B) Quantification of RNA yield from immunoprecipitated samples. (C) Assessment of RNA integrity using the TapeStation platform. (D) Hierarchical clustering heatmap depicting pairwise correlation among all RIP-Seq datasets. (E) Principal component analysis showing clustering of biological replicates and clear separation according to AKAP1 variant.

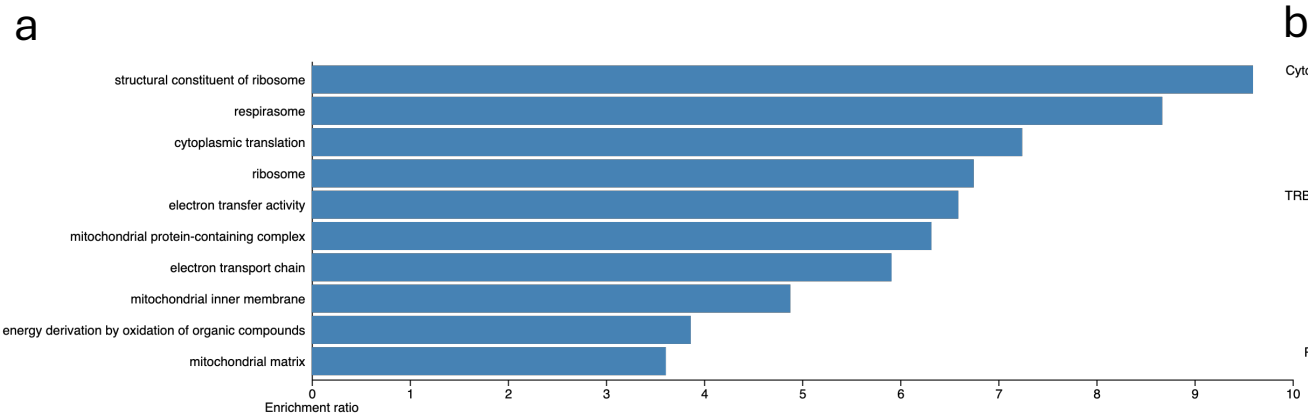

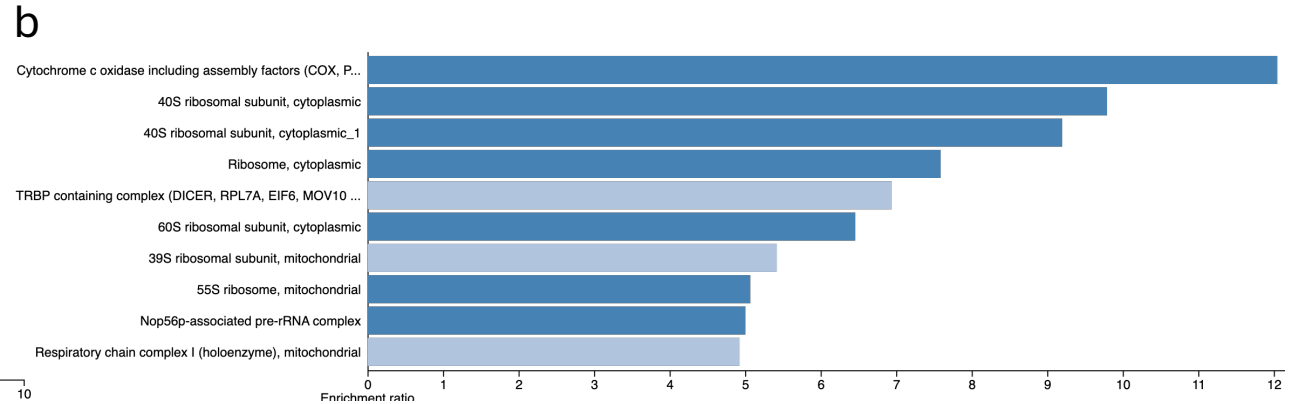

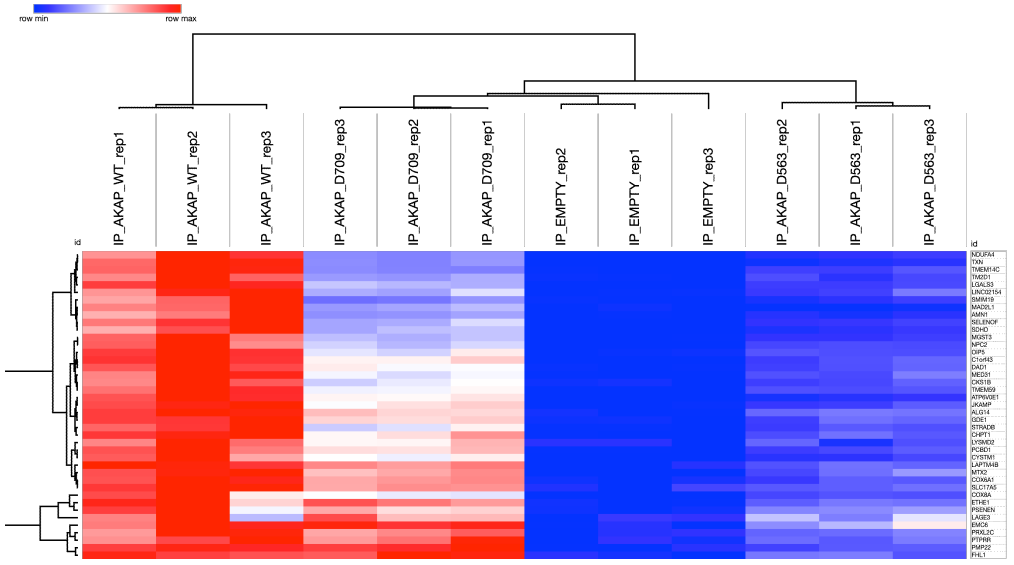

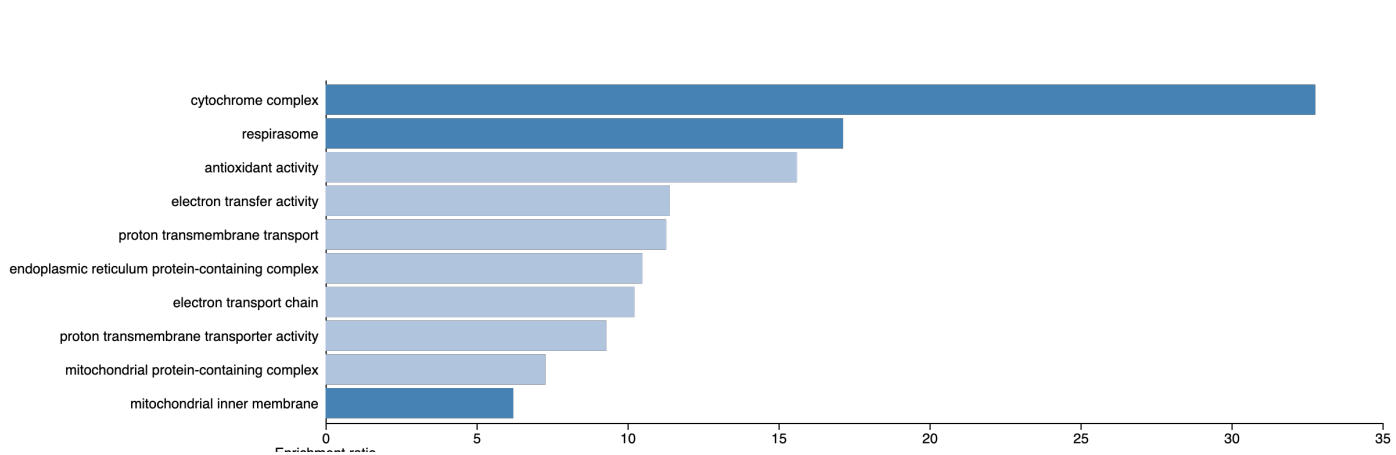

Supplementary Figure 2. (A) Hierarchical clustering heatmap showing normalized expression levels of 359 high-confidence WT AKAP1-bound transcripts across all RIP-Seq samples. Gene ontology (GO) (A) and CORUM protein complex (B) enrichment analysis of the 359 WT-specific AKAP1-associated transcripts. (C) Hierarchical clustering heatmap of normalized expression levels for 41 transcripts commonly enriched in both WT and Δ709–786 AKAP1 RIP-Seq datasets. GO (D) network enrichment analysis of the 41 shared WT/Δ709–786 AKAP1-associated transcripts. In both GO and CORUM analyses, dark blue bars represent statistically significant enrichment (FDR < 0.05), while light blue bars denote non-significant results (FDR > 0.05). Bar height indicates the enrichment ratio.

a

sample	Accession	Description	Gene
AKAP1	Q92667	A-kinase anchor protein 1, mitochondrial (	AKAP1
AKAP1	H7C5W9	P-type Ca(2+) transporter (Fragment) OS=H	ATP2A2
AKAP1	C9J2Q2	ATP synthase mitochondrial F1 complex as	ATPAF2
AKAP1	A0A024QZ91	Ataxin 2-like, isoform CRA_a OS=Homo sap	ATXN2L
AKAP1	A8K651	Complement component 1 Q subcompone	C1QBP
AKAP1	P27708	CAD protein OS=Homo sapiens OX=9606 GI	CAD
AKAP1	Q8N163	Cell cycle and apoptosis regulator protein	CCAR2
AKAP1	P06493	Cyclin-dependent kinase 1 OS=Homo sapie	CDK1
AKAP1	B4DYL7	cDNA FLJ58490, highly similar to Homo sap	CNOT1
AKAP1	A0A024RC00	CTP synthase OS=Homo sapiens OX=9606 G	CTPS2
AKAP1	Q8WVC6	Dephospho-CoA kinase domain-containing	DCAKD
AKAP1	P26196	Probable ATP-dependent RNA helicase DD	DDX6
AKAP1	Q9H072	Uncharacterized protein DKFZp586J151 OS	DKFZp586J151
AKAP1	Q6MZS5	Uncharacterized protein DKFZp686A13234	DKFZp686A13234
AKAP1	A0A024R9N6	EH-domain containing 4, isoform CRA_a OS	EHD4
AKAP1	A0A8I5KV92	Eukaryotic translation initiation factor 4 ga	EIF4G3
AKAP1	Q15717	ELAV-like protein 1 OS=Homo sapiens OX=	ELAVL1
AKAP1	P38117	Electron transfer flavoprotein subunit beta	ETFB
AKAP1	A0A384MDY5	Epididymis secretory sperm binding protei	FABP3
AKAP1	B4E2M8	cDNA FLJ61076, highly similar to UBX doma	FAF2
AKAP1	Q9NZB2	Constitutive coactivator of PPAR-gamma-li	FAM120A
AKAP1	M0R299	rRNA 2'-O-methyltransferase fibrillarin (Fr	FBL
AKAP1	Q6FI03	G3BP protein OS=Homo sapiens OX=9606 G	G3BP
AKAP1	A0A7I2V361	GRB10-interacting GYF protein 2 OS=Homo	GIGYF2
AKAP1	A0A024R0Y2	Acetyl-CoA carboxylase 1 OS=Homo sapien	hCG_30204
AKAP1	A0A024R8A7	HCG31253, isoform CRA_a OS=Homo sapie	hCG_31253
AKAP1	V9HWC7	Peroxiredoxin-6 OS=Homo sapiens OX=960	HEL-S-128m
AKAP1	V9HVZ4	Glyceraldehyde-3-phosphate dehydrogen	HEL-S-162eP
AKAP1	V9HW22	Epididymis luminal protein 33 OS=Homo sa	HEL-S-72p
AKAP1	F8W6I7	Heterogeneous nuclear ribonucleoprotein	HNRNPA1
AKAP1	A0A804HHW5	3-hydroxyacyl-CoA dehydrogenase type-2	HSD17B10
AKAP1	A8K5W7	Isoleucine--tRNA ligase OS=Homo sapiens	IARS2
AKAP1	B7Z9J8	cDNA, FLJ78862, highly similar to Isocitrate	IDH3A
AKAP1	Q9Y6M1	Insulin-like growth factor 2 mRNA-binding	IGF2BP2
AKAP1	Q71RC2	La-related protein 4 OS=Homo sapiens OX=	LARP4
AKAP1	A0A0A0MQW0	Myelin expression factor 2 OS=Homo sapie	MYEF2
AKAP1	B2RA56	Nicalin OS=Homo sapiens OX=9606 PE=2 SV	NCLN
AKAP1	P07196	Neurofilament light polypeptide OS=Hom	NEFL
AKAP1	A0A7I2V649	Polyadenylate-binding protein 1 OS=Homo	PABPC1
AKAP1	P11177	Pyruvate dehydrogenase E1 component su	PDHB
AKAP1	Q53FV0	Prohibitin (Fragment) OS=Homo sapiens O	PHB1
AKAP1	M0R2B7	DNA polymerase OS=Homo sapiens OX=96	POLD1
AKAP1	B4DZE5	DNA-directed RNA polymerase OS=Homo s	POLRMT
AKAP1	Q9BYX7	Putative beta-actin-like protein 3 OS=Hom	POTEKP
AKAP1	A0A384NPQ2	Epididymis secretory sperm binding protei	PRDX1
AKAP1	Q53HB3	Proteasome 26S ATPase subunit 1 variant (	Psmc1
AKAP1	B4DEB0	cDNA FLJ56054, highly similar to 26S protea	PSMD3
AKAP1	H0YEH2	Pumilio homolog 1 (Fragment) OS=Homo s	PUM1
AKAP1	P54136	Arginine--tRNA ligase, cytoplasmic OS=Ho	RARS1
AKAP1	E9PKZ0	60S ribosomal protein L8 (Fragment) OS=H	RPL8
AKAP1	J3QTR3	Ubiquitin-40S ribosomal protein S27a (Frag	RPS27A
AKAP1	P23396	40S ribosomal protein S3 OS=Homo sapien	RPS3
AKAP1	A0A0S2Z3I3	Solute carrier family 25 member 10 isoform	SLC25A10
AKAP1	P05141	ADP/ATP translocase 2 OS=Homo sapiens (	SLC25A5
AKAP1	O95793	Double-stranded RNA-binding protein Stau	STAU1
AKAP1	P53597	Succinate--CoA ligase [ADP/GDP-forming]	SUCLG1
AKAP1	J3KR97	Tubulin-specific chaperone D OS=Homo sa	TBCD
AKAP1	B4DE53	cDNA FLJ61213, highly similar to Tubulin-sp	TBCD
AKAP1	B4DU42	cDNA FLJ56153, highly similar to Homo sap	TBRG4
AKAP1	A0A024R983	TROVE domain family, member 2, isoform	TROVE2
AKAP1	F5H5D3	Tubulin alpha chain OS=Homo sapiens OX=	TUBA1C
AKAP1	A0A384MEE3	Tubulin beta chain OS=Homo sapiens OX=9	Tubb2b
AKAP1	B4DE77	Tubulin beta chain OS=Homo sapiens OX=9	TUBB4A
AKAP1	Q8IWP6	Tubulin beta chain OS=Homo sapiens OX=9	Tubb4b
AKAP1	Q6ZMY0	cDNA FLJ16598 fis, clone TESTI4006473, we	YTHDC2

b

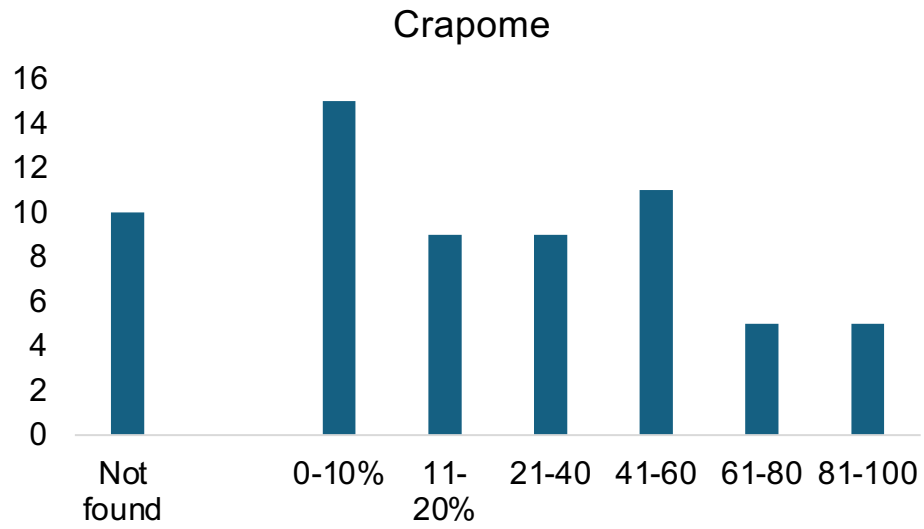

Supplementary Figure 3. (A) List of AKAP1 interacting proteins identified by proteomic analysis. Proteins identified as AKAP interactors are listed. For each protein, the Uniprot accession number, protein description and corresponding gene name, are reported. (b) Histogram showing the frequency distribution of the percentage of CRAPome studies reporting protein detection in negative controls. AKAP1 interactors identified in this study are shown as interleaved bars within each frequency bin, highlighting their prevalence across CRAPome datasets.

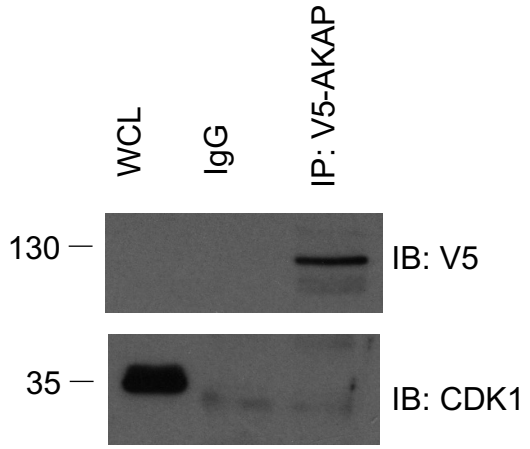

Figure S4: HeLa cells overexpressing AKAP121-V5, were lysed and immunoprecipited with anti V5 antibody. Lysates were immunoblotted with the indicated. antibodies.

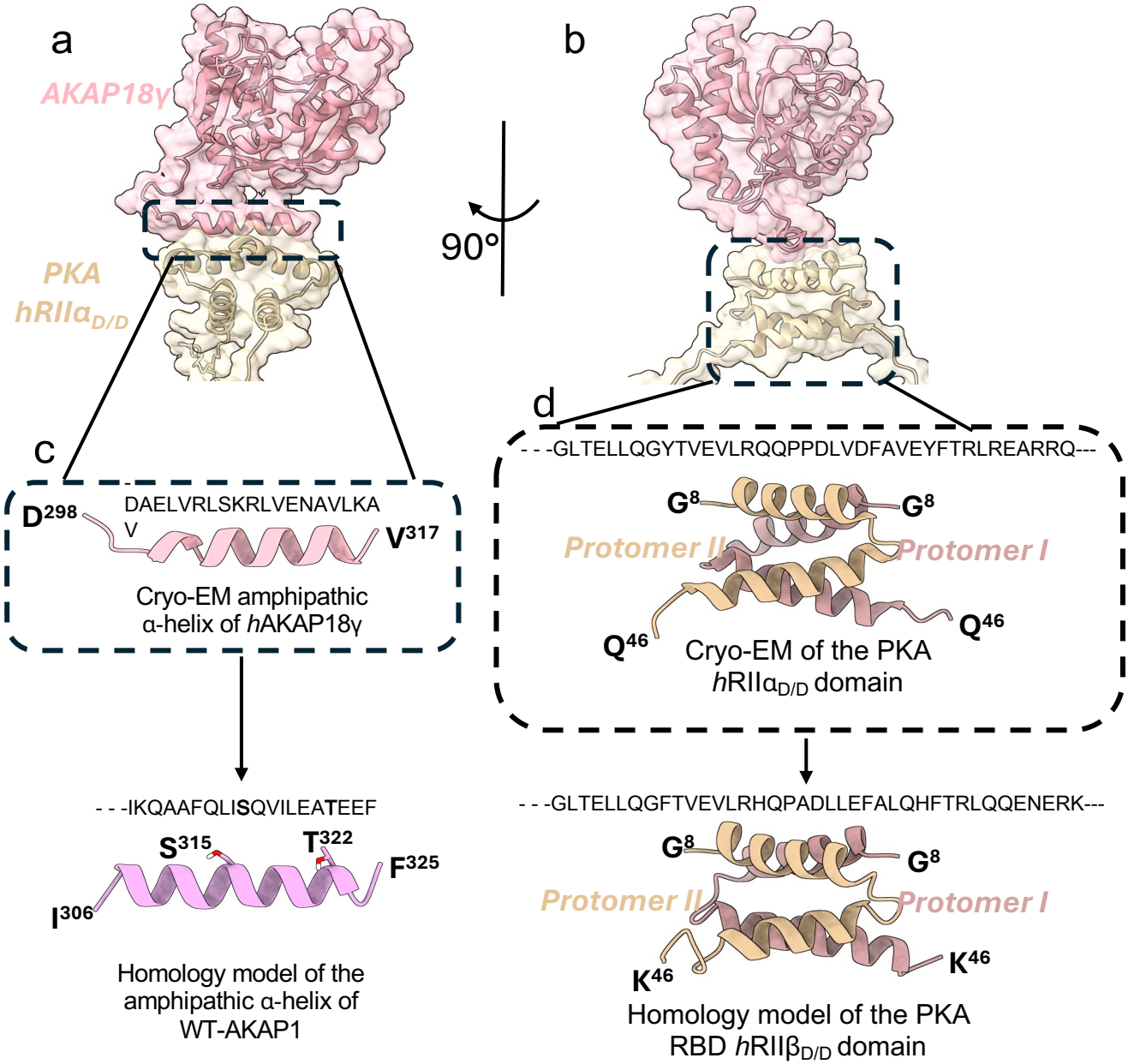

Figure S5: (A) Lateral and (B) Front view of AKAP18γ in the Cryo-EM model (PDB ID: 3J4Q); (C) Focus on the amphipathic α-helix of *h*AKAP18 and the WT-*m*AKAP1 homology model. (D) Focus on the Cryo-EM of the PKA *h*RIIα$_{D/D}$ domain and the homology model of *h*RIIβ$_{D/D}$.

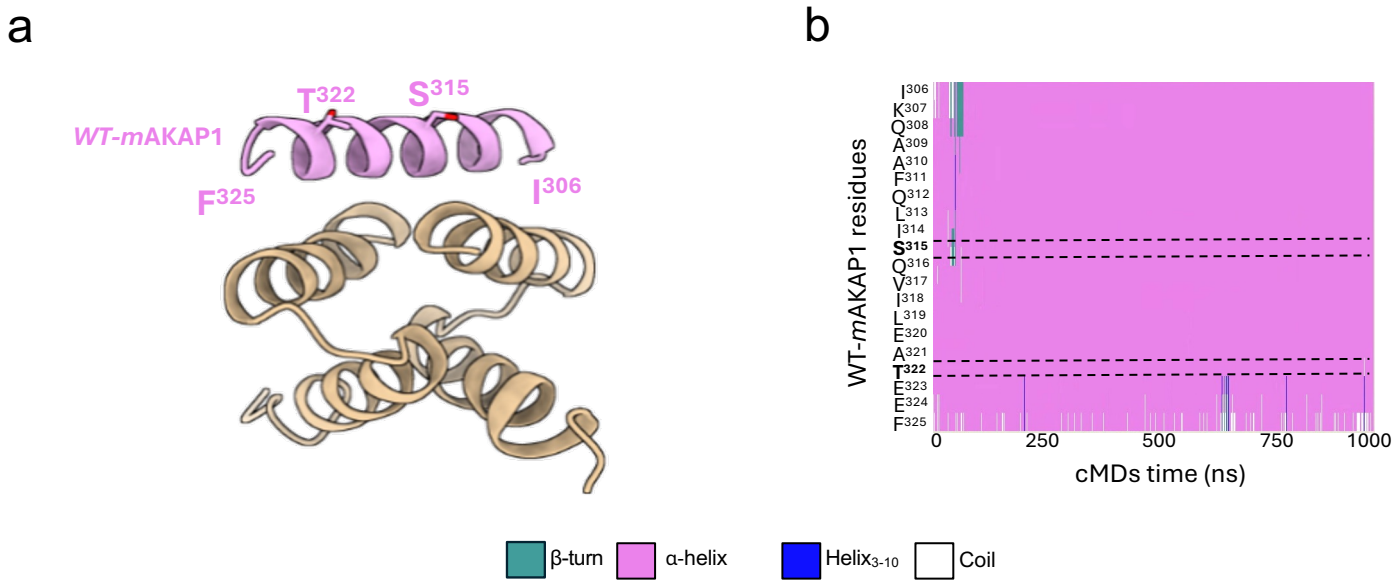

Figure S6: (a) Best cluster after 1μs of cMDs homology model of WT-mAKAP1/*h*RIIβ$_{D/D}$ interaction. (b) Per-residue secondary structure map during 1μs of cMDs of the WT-*m*AKAP1 amphipathic α-helix bound to *h*RIIβ$_{D/D}$ domain demonstrating a conserved α-helix secondary structure along the entire simulation.

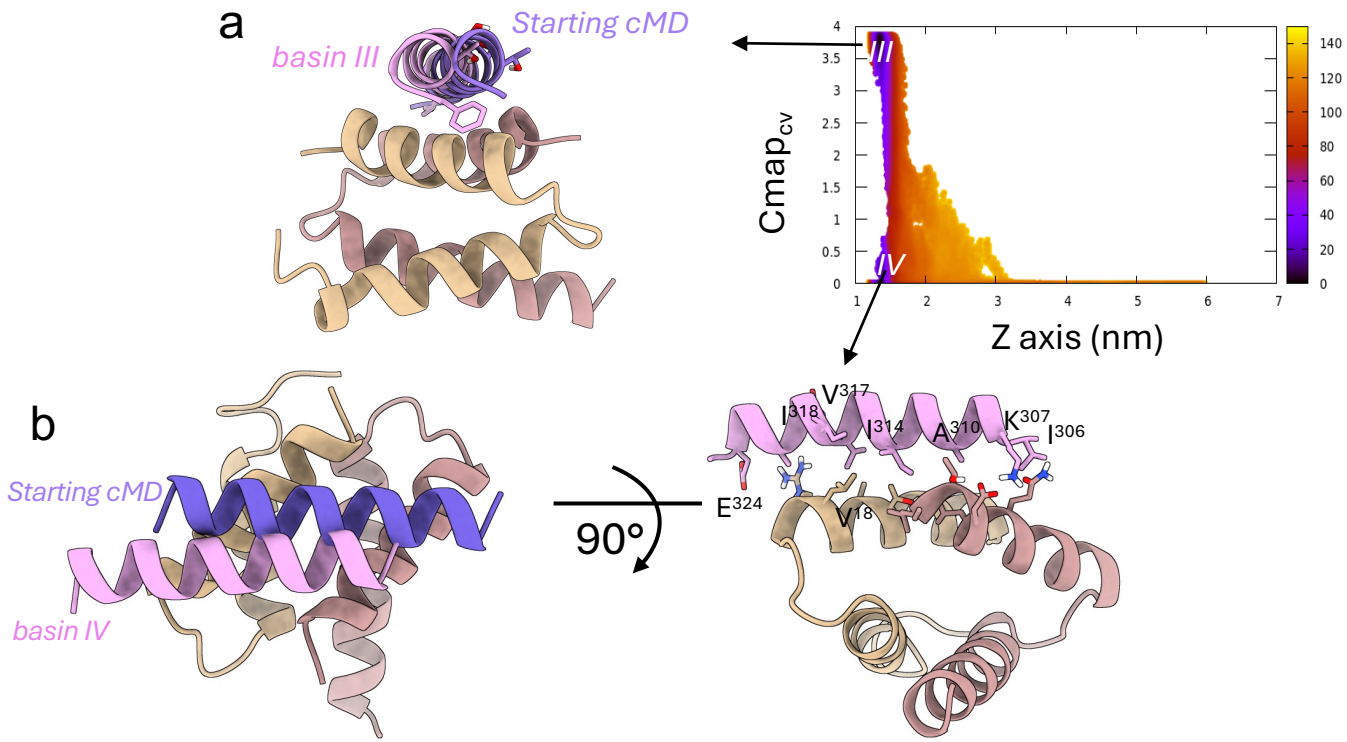

Figure S7: 2D BFES reweighted as function of funnel Z axis and cmap$_{cv}$ CVs, with the representative energetic minima extracted from basin *III* and *IV. (a)* The WT-mAKAP1 amphipathic α-helix (pink cartoon) found in basin III overlapped with that of the starting cMD conformation (violet cartoon)*; (b)* The WT-mAKAP1 amphipathic α-helix (pink cartoon) found in basin IV overlapped with that of the starting cMD conformation.

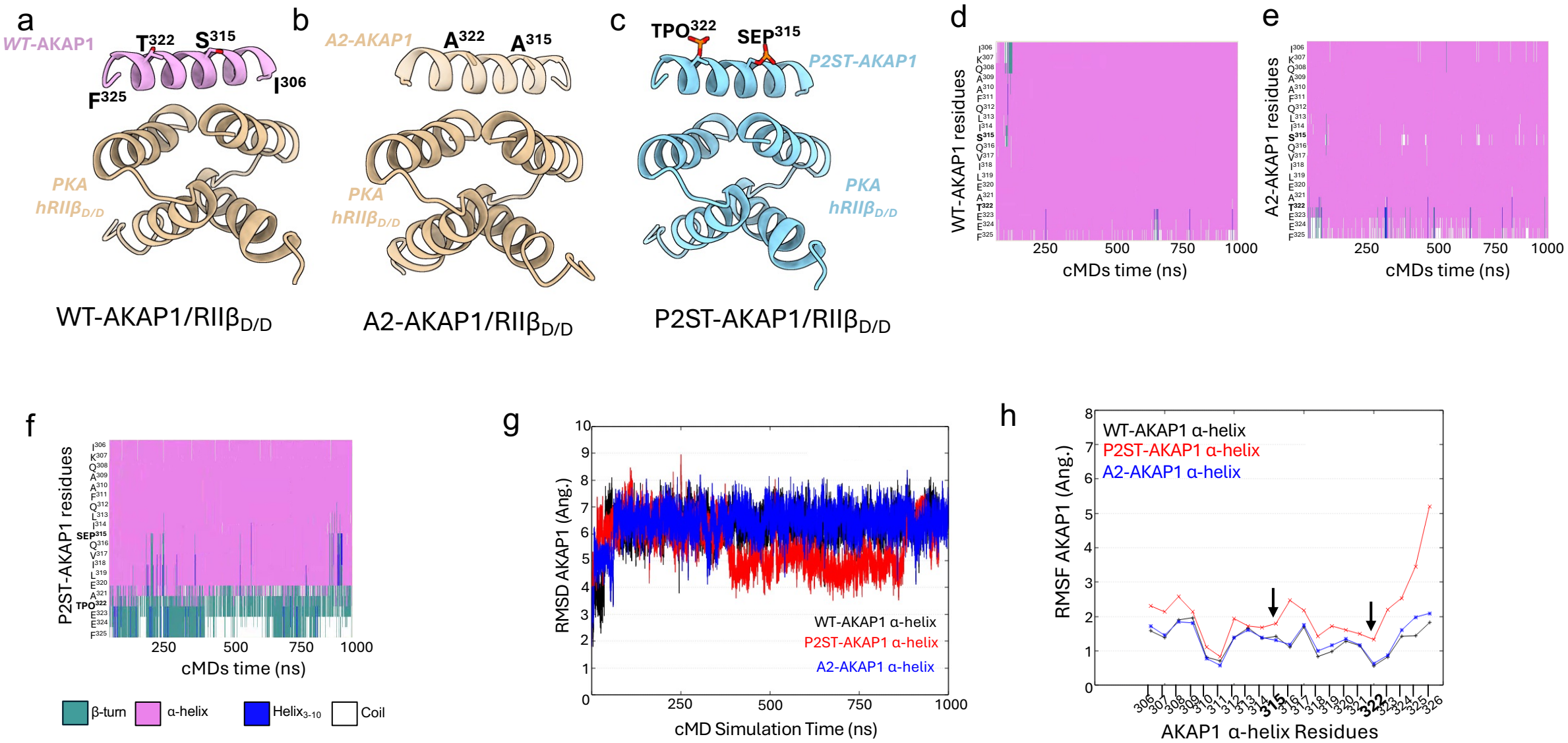

Figure S8: (a) Homology model of the wild-type WT-AKAP1/hRIIβ$_{D/D}$ system. (b) System A2/*h*RIIβ$_{D/D}$ with the S315A and T322A mutations; (c) System P2ST/*h*RIIβ$_{D/D}$ with S^{315} and T^{322} phosphorylations respectively as SEP^{315} and TPO^{322}. (d-e-f) Per-residue secondary structure map of the WT-AKAP1, A2-AKAP1 and P2ST-AKAP1 amphipathic α-helix, respectively, bound to *h*RIIβ$_{D/D}$. (g-h) Root Mean Square Deviation (RMSD) and Fluctuations (RMSF), respectively, of the AKAP1 helix.

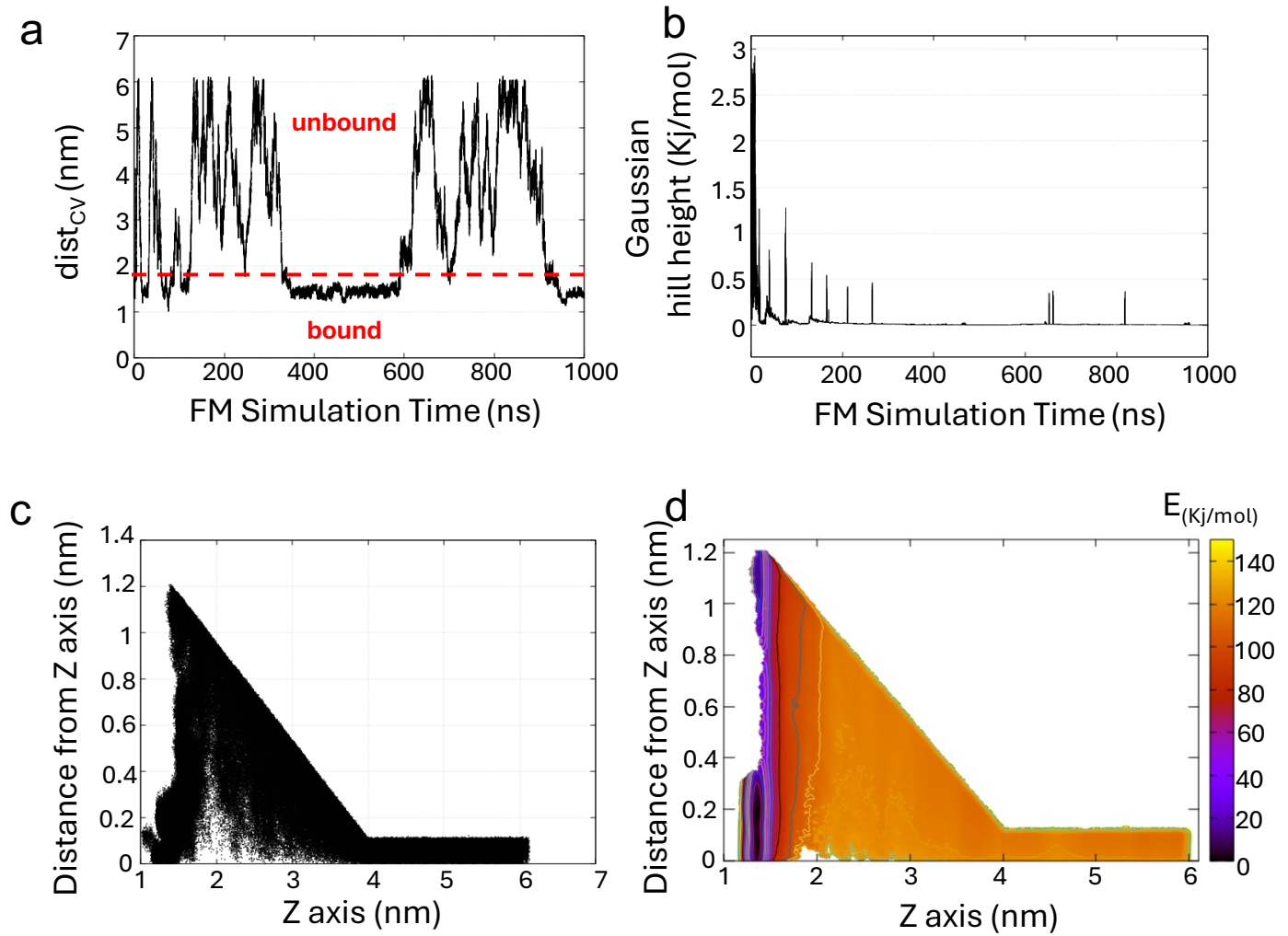

Figure S9: (a) Multiple recrossing bound/unbound events of the WT-AKAP1 amphipathic α-helix from the PKA *h*RIIβ$_{D/D}$ during FM simulation. (b) Decrease of the Gaussian height during the FM simulation according to the Well-Tempered algorithm. (c) WT-AKAP1 COM exploration within the funnel space. (d) 3D FES reweighted as function of projection on the z axis and distance from z axis of the COM of the WT-AKAP1 amphipathic α-helix.

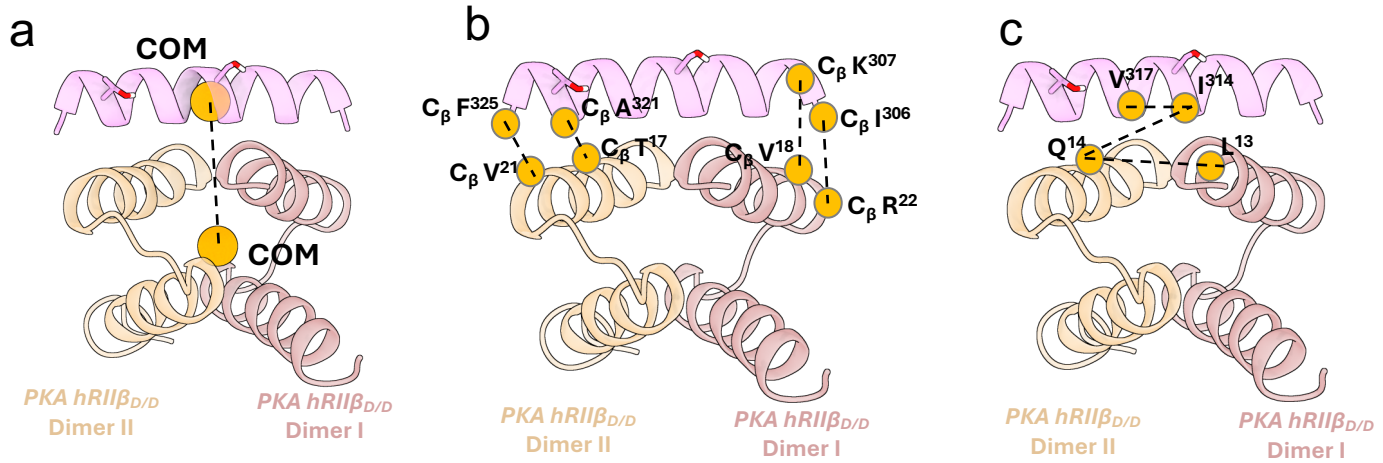

Figure S10: Representation of (a) The Center of Mass (COM) used to define the biased $dist_{cv}$; (b-c) Monitored $cmap_{cv}$ and $tors_{cv}$, respectively, used to reweright the Free-Energy Surface.

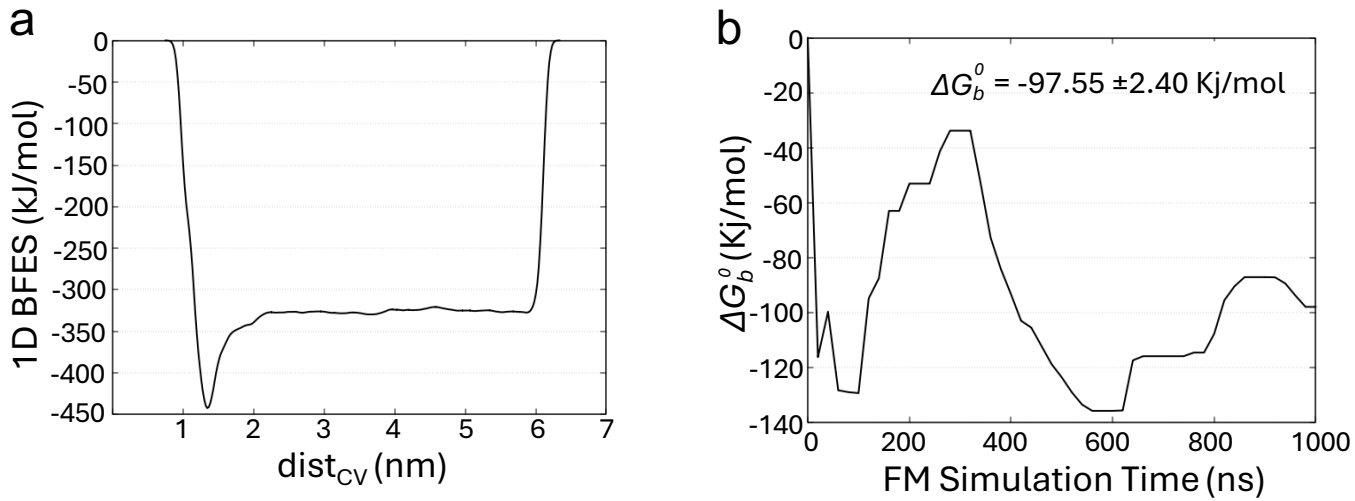

Figure S11: (a) 1D BFES of biased $dist_{cv}$ (b) Protein–Protein binding free energy difference between the bound and unbound state.